Recent Insights into the Physics of the Sun and Heliosphere:
Highlights from SOHO and Other Space Missions
IAU Symposium, Vol. 203, 2001
P. Brekke, B. Fleck, and J. B. Gurman eds.

Spectroscopic Features in the EUV Emission of a M8 Flare Observed by SUMER

W. Curdt[1], E. Landi[1,2], U. Feldman[2], D. Innes[1], B. Dwivedi[1,3], and K. Wilhelm[1]

[1]*Max-Planck-Insitut für Aeronomie, 37191 Katlenburg-Lindau, Germany*

[2]*E.O.Hulburt Center for Space Res., NRL, Washington DC 20375, USA*

[3]*Department of Applied Physics, Banaras Hindu University, Varanasi-221005, India*

Abstract.

A flare of size M8 occurred while SUMER was recording a spectral scan above the active region NOAA 8537 at the west limb. We recorded spectra during the pre-flare phase, at flare onset, and during the decay phase of this main flare in a series of events. More than 60 flare lines were identified during this observation, which include Fe XVIII - Fe XXIII lines that provide evidence of 10^7 K plasmas. We also recorded lines from He-like ions, such as Ne IX, Na X, Mg XI, and Si XIII. Accurate wavelength measurements of such lines are of interest in basic atomic physics studies. Using plasma diagnostic techniques, we investigated the temporal evolution of the electron densities and temperatures during the event.

1. Introduction and Data Acquisition

On May 9, 1999 the SOHO/SUMER spectrograph recorded EUV spectra from a bright active region located above the west limb (cf., Fig. 1). During the 6.7 hours of observations the instrument obtained two complete spectra spanning the entire SUMER wavelength range from 500 Å to 1600 Å in 43 Å sections. The GOES-8/10 records show eruptions of several flares of different sizes on the Sun from about 12:00 UT onwards. A flare of size C5.1 occurred at 16:09, when the instrument recorded the spectrum around 980 Å. The instrument was still continuing the first spectral scan when at ≈17:53 a M7.6 flare erupted in the observed active region. The X-ray flux peaked at ≈18:07 and gradually decayed over the next three hours. At flare onset the detector recorded spectra near 1395 Å, while advancing towards longer wavelengths, and reached 1450 Å at the time of peak X-ray flux. In a companion paper based on SUMER, EIT, Yohkoh-SXT, and MICA coronagraph data Innes (2000) has demonstrated that the flare onset occurred on the sunward side of the SUMER slit position, from where it rapidly expanded to the site observed by the spectrometer. The spectra that were acquired during this flare contained the hottest high-resolution astrophysical spectral recordings ever made in the wavelength range from 500 Å to 1600 Å.

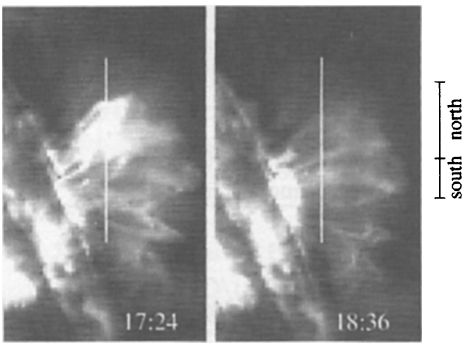

Figure 1. EUV images of the active region loop system before and after the flare onset taken by EIT in the Fe XII/195 Å channel (characteristic temperature about 10^6 K). The position of the SUMER slit is indicated. The bright loops in the upper portion of the slit have disappeared during the event.
(Courtesy EIT consortium)

2. The Flare Spectrum

The spectra recorded on May 9, 1999 contain a large number of spectral lines emitted by hot ($T_e \geq 3 \cdot 10^6$ K) plasmas and are dominated by bright lines from forbidden transitions. Interestingly, even prior to the onset of the main flare hot-plasma lines are present in our spectrum. Some of the lines have previously been observed in solar or laboratory spectra, the latter emitted by Tokamak plasmas or by beam-foil sources, but some of the flare lines have never been identified before. We achieved a pixel-to-wavelength calibration with uncertainties from 10 mÅ to 50 mÅ depending on the availality of cool emission lines in the exposure. A list of all high-temperature lines detected in the flare spectra is given in Table 1 in Feldman et al. (2000), which includes the line identifications with uncertainty estimates and, if available, the previously most accurately derived wavelengths, references to the quoted values and the temperatures of maximum fractional abundance of the emitting ions.

In our spectrum we see isoelectronic sequences from helium to neon and also H-like transitions from the He^+ Balmer series. $1s2s\ ^3S_1$–$1s2p\ ^3P_{0,2}$ transitions of He-like species are of particular interest for theoretical physics: accurate wavelength measurements of the transitions are used as benchmarks for comparisons with calculations of both relativistic and quantum-electrodynamical effects in 3-body systems (Drake 1988). We have identified He-like lines from Ne^{8+} to Si^{12+} and believe that our measurements of these wavelengths are the first to be done from collisional astrophysical plasmas (cf., Curdt et al. 2000). We also see Be-like ions up to Fe^{22+}, B-like ions up to Fe^{21+}, C-like ions up to Ni^{22+}, N-like ions up to Co^{20+}, O-like ions up to Ni^{20+}, F-like ions up to Ni^{19+}, and Ne-like ions up to Ni^{18+}.

3. High-temperature Density and Temperature Diagnostic

The intensity of many of the lines can be used to determine the electron densities, electron temperatures, emission measure distributions, mass motions and the state of ionization equilibrium of the plasmas. We have used the methods outlined by Feldman et al. (2000) to measure the electron density and temperature summarized in Table 1, where we distinguish among three density groups, which have an almost identical signature along the slit. We have used

https://doi.org/10.1017/S0074180900219244 Published online by Cambridge University Press

Table 1. Electron temperatures versus time for three density groups at two different sites

time	log T_e /K		ratio
seconds	south	north	line 1 / line 2
	Group 1: log n_e/cm^{-3} = 9.4 - 9.45		
4373/4684	6.27 ± 0.05	6.28 ± 0.05	Ca XIV 1190(2)/Ca XIII 1133
4684/4996	6.34 ± 0.05	6.34 ± 0.05	Ca XIII 1133/Ca XIV 1159(2)
4996	6.33 ± 0.05	6.33 ± 0.05	Ca XIII 1133/Ca XIV 1159(2)
4996/5309	6.30 ± 0.05	-	Ca XIII 1133/Ca XIV 1159(2)
5309/7203	6.35 ± 0.05	-	Ca XIV 1291 /Ca XIII 1297(2)
7830/8769	6.31 ± 0.06	6.32 ± 0.07	Ar XII 1340(2)/Ar XI 1392
16367/16673	6.36 ± 0.05	-	Ca XIV 1190(2)/Ca XIII 1133
16673/16985	6.36 ± 0.05	6.33 ± 0.05	Ca XIII 1133/Ca XIV 1159(2)
16985	6.35 ± 0.05	6.31 ± 0.05	Ca XIII 1133/Ca XIV 1159(2)
16985/17298	6.33 ± 0.05	6.29 ± 0.05	Ca XIII 1133/Ca XIV 1159(2)
17298/19193	6.35 ± 0.05	6.33 ± 0.05	Ca XIV 1291 /Ca XIII 1297(2)
19819/20758	6.34 ± 0.08	6.30 ± 0.07	Ar XII 1340(2)/Ar XI 1392
	Group 2: log n_e/cm^{-3} = 11.1		
624/1560	6.67 ± 0.08	6.62 ± 0.07	Ti XVI 861/ Ti XV 919
937/1872	6.62 ± 0.07	6.62 ± 0.08	Ti XVI 861/ Ti XV 919
2185/4996	6.66 ± 0.13	6.72 ± 0.13	Fe XVIII 974/Fe XVII 1153
2498/5309	6.62 ± 0.13	6.68 ± 0.12	Fe XVIII 974/Fe XVII 1153
9083/10021	6.60 ± 0.08	6.55 ± 0.08	Cr XVI 1410/Cr XVII 1481
9083/10334	6.63 ± 0.08	6.51 ± 0.07	Cr XVI 1410/Cr XVII 1481
12613/13548	6.64 ± 0.08	6.57 ± 0.07	Ti XVI 861/ Ti XV 919
12925/13861	6.62 ± 0.08	6.61 ± 0.09	Ti XVI 861/ Ti XV 919
20758/22010	6.46 ± 0.07	6.61 ± 0.08	Cr XVI 1410/Cr XVII 1481
21071/22323	6.49 ± 0.07	6.63 ± 0.08	Cr XVI 1410/Cr XVII 1481
	Group 3: log n_e/cm^{-3} = 12.0 - 13.0		
312	$\leq$ 6.7	6.74 ± 0.03	Fe XX 821/ Fe XXII 845
624	$\leq$ 6.7	6.75 ± 0.03	Fe XX 821/ Fe XXII 845
624/3746	$\leq$ 6.7	-	Fe XX 821/ Fe XXIII 1079
624/3746	$\leq$ 6.7	-	Fe XXII 845/ Fe XXIII 1079
3746/5309	$\leq$ 6.7	-	Fe XXIII 1079/Fe XXI 1171(2)
8143	6.88 ± 0.08	-	Fe XXI 1354/Fe XX 1358(2)
8143/8455	6.94 ± 0.09	-	Fe XXI 1354/Fe XX 1358(2)
9396/11275	6.84 ± 0.08	7.16 ± 0.13	Fe XX 1443(2)/Fe XXI 1572(2)
11588	-	-	Fe XXI 1572(2)/Fe XX 1586
12301	6.84 ± 0.04	6.93 ± 0.04	Fe XX 821/ Fe XXII 845
12613	6.86 ± 0.04	6.93 ± 0.05	Fe XX 821/ Fe XXII 845
12613/15736	-	-	Fe XX 821/ Fe XXIII 1079
12613/15736	-	-	Fe XXII 845/ Fe XXIII 1079
16049/17298	-	-	Fe XXIII 1079/ Fe XXII1171(2)
20132	6.73 ± 0.06	6.86 ± 0.08	Fe XXI 1354/Fe XX 1358(2)
20132/20444	-	6.92 ± 0.09	Fe XXI 1354/Fe XX 1358(2)
21698/23577	-	6.74 ± 0.06	Fe XX 1443(2)/Fe XXI 1572(2)
23577	-	-	Fe XXI 1572(2)/Fe XX 1586

https://doi.org/10.1017/S0074180900219244 Published online by Cambridge University Press

K XIII (994/945), Ar XII (1054/1018), Ca XV (1098/555, 555/1375) and Fe XXI (585/1354) for this exercise. We give temperature values for two spatial positions along the slit (cf., Fig.1), where we averaged over the indicated pixels. The errors are typically 0.04 to 0.07 DEX. The first column indicates the minutes from start-of-observation for both of the lines taken into account. The flare onset occurs at ≈9,200 seconds on this scale.

4. Discussion and Outlook

Interestingly, there is almost no temperature difference found between both positions and there is also no temperature change observed during flare onset for density groups 1 and 2. This clearly indicates that this plasma is not affected by the flare: temperatures are already high and they do not go up during the flare. Only in the 'north' section of density group 3 a temperature increase is seen during and after the event. Work is in progress to investigate the implications for flare models of this unexpected results. The lines emitted by ions from many different elements can also be used to determine the relative elemental abundances in hot astrophysical plasmas. This will be presented in a future communication.

Acknowledgments. SUMER is financially supported by DLR and international partners. SOHO is a project of international co-operation between ESA and NASA.

References

Curdt, W., Landi, E., Wilhelm, K., & Feldman, U. 2000, Phys.Rev.A **62**, 022502

Drake, G.W.F. 1988, Can. J. Phys. **66**, 586

Feldman, U., Curdt, W., Landi, E., & Wilhelm, K. 2000, ApJ **544**, in press

Innes, D. 2000, this volume